Optical polarization in mono and bilayer MoS_2

Youngsin Park [a], Nannan Li [a], Christopher C. S. Chan [b], Benjamin P. L. Reid [b], Robert A. Taylor [b,*], Hyunsik Im [c,*]

[a] School of Natural Science, Ulsan National Institute of Science and Technology (UNIST), Ulsan 44919, Korea

[b] Clarendon Laboratory, Department of Physics, University of Oxford, Oxford, OX1 3PU, UK

[c] Division of Physics and Semiconductor Science, Dongguk University, Seoul 04620, Korea

ABSTRACT

Optical anisotropy in monolayer- and bilayer-MoS_2 was investigated by polarization resolved photoluminescence measurements. The photoluminescence of monolayer-MoS_2 is found to be partially polarized at 4.2 K and maintains this polarization characteristic up to room temperature, while the photoluminescence of bilayer-MoS_2 shows no obvious polarization. This polarization anisotropy is due to strain effects at the interface between the MoS_2 layer and the SiO_2 substrate, causing symmetry breaking of the MoS_2 charge distribution. Calculations using density functional theory of the electron density distribution of the monolayer- and bilayer-MoS_2 in the in-plane direction are also presented, giving support to our qualitative analysis.

Keywords: MoS_2; photoluminescence; polarization; density functional theory; charge distribution

* Corresponding author

E-mail addresses: Robert.taylor@physics.ox.ac.uk (R.A.T), hyunsik7@dongguk.edu (H.I)

1. Introduction

Layered two-dimensional (2D) materials have been the center of attention for applications in next-generation nanoelectronic technology because of their unusual physical and electronic properties. Although graphene is a promising material due to its rich physics and relatively well studied chemical synthesis [1-3], pristine graphene has no bandgap, which is a disadvantage for applications in electronic and optical devices. 2D MoS_2, on the other hand, exhibits a bandgap of 1.2~1.9 eV depending on the layer thickness [4-8], and has thus drawn a considerable amount of attention as a potential material for optoelectronic devices. That is to say, a monolayer of MoS_2 (1L-MoS_2) is a direct gap semiconductor with a band gap of 1.8~1.9 eV at the K-points of the 2D hexagonal Brillouin zone, whereas bulk MoS_2 is an indirect semiconductor with a band gap of ~1.2 eV. There has been much interest generated in studying the characteristic optical properties of MoS_2 using photoluminescence (PL) measurements [7-9] as well as the valleytronics related to its 2D symmetry [10-14]. The fascinating electronic properties of this material have already led to the development of some interesting novel devices [16,17]. Moreover, valleytronic devices such as phototransistors and FETs for sensors have also been demonstrated based on 1L-MoS_2 [15-20]. Recently, valley-based polarization has been shown in 1L-MoS_2 by selectively exciting the degenerate K and K′ states with right and left circularly polarized light [11-15], and also by electrical control in bilayer MoS_2 (2L-MoS_2) [16], demonstrating the material's potential for valley-based electronics. The study of the physical properties of atomically thin MoS_2 is essential in understanding its optical transitions. However, due to their inherent 2D nature, the electrical and optical properties of 1L- and 2L-MoS_2 can be greatly affected by their surfaces and the MoS_2/substrate interface. It is therefore

important to understand how such interfaces can affect the optical and electronic features of the material.

In this paper, we demonstrate optical anisotropy of 1L- and 2L-MoS_2 by using polarization resolved PL. This polarization anisotropy in the 1L-MoS_2 is shown to arise from strain effects at the interface between the MoS_2 layer and the SiO_2 substrate. Density functional theory (DFT) calculations were performed to determine the electron density distribution of the 1L- and 2L-MoS_2 in the in-plane direction. The in-plane optical anisotropy could be used to produce polarization- sensitive photodevices that are useful for optoelectronic circuits, optical switches and interconnects, optically driven quantum dot computing and high-resolution near-field imaging.

2. Experimental

The 1L- and 2L-MoS_2 flakes were prepared on a SiO_2/Si substrate by mechanical exfoliation from 2H-MoS_2. In order to confirm the number of atomic layers, the MoS_2 flakes were characterized by micro-Raman spectroscopy. For the low temperature PL measurements, the sample was mounted in a continuous-flow helium cryostat, allowing the temperature to be controlled accurately from 4.2 K to room temperature and the optical luminescence properties were characterized by using micro-photoluminescence (μ-PL). A CW linearly polarized solid-state laser operating at a wavelength of 532 nm was used for the excitation of the MoS_2 flake. A 100× (NA 0.7) objective was held above the cryostat focusing the incident laser beam to a spot size of ~0.8 μm^2 and also to collect the emitted luminescence from the same spot. The polarization properties of the MoS_2 flake emission were analyzed by rotating a linear polarizer over a range of 360°. The measured PL polarization is corrected to compensate for the depolarization effects caused by the system, and for any induced polarization caused by the

spectrometer or mirrors. All the calculations were performed by using the Vienna *ab initio* simulation package (VASP). Project augmented wave (PAW) pseudopotentials within a 440 eV energy cutoff were used for modeling ion cores. The exchange-correlation energy was calculated with a generalized gradient approximation (GGA) functional of the Perdew-Burke-Ernzerhof (PBE) type. Furthermore, van der Waals density functional theory (vdW-DFT) with an optB86b functional was used to include dispersion interactions between the MoS_2 layers and SiO_2 surface.

3. Results and discussion

Figure 1(a) shows the optical microscopy image of the mechanically-exfoiliated MoS_2 flake on a SiO_2 substrate. The flake consists of 1L and 2L-MoS_2 regions. In order to confirm the number of MoS_2 layers, Raman spectroscopy measurements (see Fig. 1(b)) were undertaken at the two different contrast regions shown in Fig. 1(a). In the MoS_2 material, the two prominent Raman bands measured were assigned as in-plane E^1_{2g} at 385.4 cm^{-1} and out-of-plane A_{1g} modes at 402.3 cm^{-1}, showing systematic frequency progressions as a function of thickness. It is well known that the frequency difference between these two bands serves as and indictor of the exact number of layers. Frequency differences at the upper semi-transparent and bottom dark regions are 17.77 cm^{-1} and 21.01 cm^{-1} corresponding to 1L- and 2L-MoS_2, respectively. These values are in good agreement with the values in the literature **[**20**]**.

Figures 2(a) and (b) show the μ-PL spectra of the 1L- and 2L-MoS_2 measured at 4.2 K and 292 K, respectively. A prominent PL peak can be identified at ~1.869 eV for 1L-MoS_2 and 1.876 eV for 2L-MoS_2 at 4.2 K. The PL intensity and the emission energy of the 2L-MoS_2 are more intense and higher than those of the 1L-MoS_2 at low temperature. However, the opposite behavior is seen at room temperature, which is

consistent with previous results [6]. We should also consider the relationship of the emission energy and the physical nature of the MoS_2/SiO_2 interface, which may cause different strain in 1L- and 2L-MoS_2. We do not fully understand this phenomenon. It is known that the PL spectrum and intensity of atomically thin MoS_2 are affected by defects and the substrate as well as by the layer number [21-24]. Thus, we presume that complex, temperature-dependent interplay between these factors is linked to this observation. This will be reported elsewhere.

Figures 3(a) and 3(b) present polarization-angle resolved PL spectral mapping of the 1L- and 2L-MoS_2 at 4.2 K, respectively. The polarization angles in Figure 3 are relative to an arbitrary direction (where our linear analyzer started measuring). Both 1L- and 2L-MoS_2 show a polarization anisotropy in the PL at 4.2 K. In addition, it can be seen by comparing Figures 3(a)~(d), that the emission energy peaks and intensity for the 1L- and 2L- MoS_2 are consistent with the results presented in Figure 2. The entire peak intensity was integrated and plotted against the polarization angle of the linear analyzer. In order to characterize any systematic errors, an unstrained AlGaAs/GaAs multi quantum well was measured with the same system parameters to serve as a reference. The measured MoS_2 data was subsequently calibrated with this reference in order to remove systematic errors arising from any optical misalignment. The calibrated intensity variations for both the sampled areas at 4.2 K and 292 K were presented in Figure 4. It is apparent that the 1L-MoS_2 shows a certain degree of polarization anisotropy in its PL spectra at both 4.2 K and 292 K. Increasing the temperature is found to decrease the degree of polarization of the 1L area slightly. For the 2L areas, however, the results show very slight polarization anisotropy at 4.2 K compared to that seen at 292 K.

Figure 4(a) shows a polar plot comparing the PL intensities of the 1L-MoS_2 at 4.2 K and 292 K at the same analyzer angles. Differences in the PL polarization can be seen clearly in this plot as the polarizers are rotated. The degree of linear polarization (DLP), defined by $(I_{max}-I_{min})/(I_{max}+I_{min})$, in the measured angular range is found to be ~22 % for the 1L-MoS_2 at 4.2 K. This decreases slightly at room temperature within error boundaries. However, the DLP of the 2L-MoS_2 almost disappears, as shown in Fig. 4(b). The PL from the 2L-MoS_2 is considered linearly unpolarized taking into account experimental fluctuations. The PL from the 1L- and the 2L-MoS_2 differs not only in emission energy, intensity and but also polarization. The temperature dependent behavior of this effect leads us to believe that this polarization anisotropy may be caused by strain existing at the interface between the MoS_2 layer and SiO_2 substrate.

In an attempt to understand the polarization dependent PL, DFT calculations were performed for the 1L- and 2L-MoS_2 on the SiO_2 substrate by using projector augmented wave pseudopotentials with a plane-wave basis set as implemented in the Vienna *ab-initio* simulation package (VASP) [25]. Figure 5(a) shows the calculated structure of the 2L-MoS_2 including the SiO_2 substrate. The lattice mismatch is about 3.5% between above two structures. The structures were optimized until all of the forces were smaller than 0.025 eV/Å and the energy convergence reached the criterion 10^{-7} eV. Contour maps of the charge density are shown in Figures 5(b) and 5(c). The corresponding position of the charge density contour map is also shown in the geometry of the system. The conduction-band minimum and valence-band maximum at the K-point was derived from (Mo-) atomic *d* orbitals. When subject to strong quantum confinement in a non-spherical symmetry, they may give rise to both electron and hole levels with strongly anisotropic charge distribution, which in turn will produce polarization-dependent transitions. Figures 5(b) and 5(c) show the calculated electron density distribution at

the interfaces between SiO_2 and 1L-MoS_2 and between 1L-MoS_2 and 2L-MoS_2 respectively. A large difference can be seen in terms of the spatial distribution of the electron density in these two systems. As shown in Fig. 5(b), in the middle of 1L-MoS_2 and SiO_2, the electron density is mainly distributed around the S atom, and it is almost zero near the Mo position, which results in symmetry breaking of the charge distribution. For the 2L-MoS_2 system shown in Fig. 5(c), however, the electron density distribution does not show much difference between S and Mo atoms. The 1L-MoS_2 has an inversion asymmetry [4,12,26], while the 2L-MoS_2 has an inversion symmetry [4,10,13] in the unit cell as the valley dependent optical selection rule is not allowed. However, the inversion symmetry can be broken by applying an electric field perpendicular to the bilayer, which leads to a potential difference between the two layers [14].

4. Conclusion

In summary, we have demonstrated optical anisotropy in the excitonic PL of 1L- and 2L-MoS_2. We find that there exists a degree of polarization of the PL in 1L-MoS_2 at low temperatures. The polarization of the 1L-MoS_2 is retained up to room temperature. To shed light on this behavior, DFT calculations were performed for both 1L- and 2L-MoS_2 on SiO_2. The charge density distribution between 1L-MoS_2 and SiO_2 substrate shows symmetry breaking in the in-plane direction. The internal field caused by this symmetry breaking can alter the PL polarization in relevant direction. Clear understanding of electronic structures in 1L- and 2L-MoS_2 through photo-excited carriers is important in designing transparent semiconducting MoS_2 monolayer-based optoelectronic devices as well as in exploring novel mesoscopic physics in this emerging 2D system.

Acknowledgments

This research was supported by Basic Science Research Program through the National Research Foundation of Korea (NRF) funded by the Ministry of Education, Science and Technology (Grant No. 2015R1D1A1A01058332, 2016R1A6A1A03012877, 2015M2A2A6A02045252, and 2015R1A2A2A01004782).

References

1. K. S. Novoselov, A. K. Geim, S. V. Morozov, D. Jiang, M.I. Katsneison, I.V. Grigorieva, S.V. Dubonos, A.A. Firsov, Two-dimensional gas of massless Dirac fermions in graphene, Nature 438 (2005) 197–200.
2. Y. Zhang, Y. W. Tan, H. L. Stormer, P. Kim, Experimental observation of the quantum Hall effect and Berry's phase in graphene, Nature 438 (2005) 201–204.
3. K. S. Kim, Y. Zhao, H. Jang, S. Y. Lee, J. M. Kim, K. S. Kim, J. H. Ahn, P. Kim, J. Y. Choi, B. H. Hong, Large-scale pattern growth of graphene films for stretchable transparent electrodes, Nature 457 (2009) 706–710.
4. T. Cheiwchanchamnangij, W. R. L. Lambrecht, Quasiparticle band structure calculation of monolayer, bilayer, and bulk MoS_2, Phys. Rev. B 85 (2012) 205302.
5. W. S. Yun, S. W. Han, S. C. Hong, I. G. Kim, J. D. Lee, Thickness and strain effects on electronic structures of transition metal dichalcogenides: 2H-MX_2 semiconductors (M = Mo, W; X = S, Se, Te), Phys. Rev. B 85 (2012) 033305.
6. K. F. Mak, C. Lee, J. Hone, J. Shan, T. F. Heinz, Atomically thin MoS_2: A new direct-gap semiconductor, Phys. Rev. Lett. 105 (2010) 136805.

7. A. Splendiani, L. Sun, Y. Zhang, T. Li, J. Kim, C.Y. Chim, G. Galli, F. Wang, Emerging photoluminescence in monolayer MoS_2, Nano Lett. 10 (2010) 1271−1275.
8. T. Korn, S. Heydrich, M. Hirmer, J. Schmutzler, C. Schuller, Low-temperature photocarrier dynamics in monolayer MoS_2, Appl. Phys. Lett. 99 (2011) 102109.
9. G. Eda, H. Yamaguchi, D. Voiry, T. Fujita, M. Chen, M. Chhowalla, Photoluminescence from chemically exfoliated MoS_2, Nano Lett. 11 (2011) 5111−5116.
10. K. F. Mak, K. He, J. Shan, T. F. Heinz, Control of vally polarization in monolayer MoS_2 by optical helicity, Nat. Nanotech. 7 (2012) 494−498.
11. H. Zeng, J. Dai, Y. Wang, D. Xiao, X. Cui, Valley polarization in MoS_2 monolayers by optical pumping, Nat. Nanotech. 7 (2012) 490−493.
12. D. Xiao, G.B. Liu, W. Feng, W. Xu, W. Yao, Coupled spin and valley physics in monolayers of MoS_2 and other group-VI dichalcogenides, Phys. Rev. Lett. 108 (2012) 196802.
13. T. Cao, G. Wang, W. Han, H. Ye, C. Zhu, J. Shi, Q. Niu, P. Tan, E. Wang, B. Liu, J. Feng, Valley-selective circular dichroism of monolayer molybdenum disulphide, Nat. Comm. 3 (2012) 887.
14. S. Wu, J. S. Ross, G. B. Liu, G. Aivazian, A. Jones, Z. Fei, W. Zhu, D. Xiao, W. Yao, D. Cobden, X. Xu, Electrical tuning of valley magnetic moment through symmetry control in bilayer MoS_2, Nat. Phys. 9 (2013) 149−153.
15. G. Sallen, L. Bouet, X. Marie, G. Wang, C.R. Zhu, W.P. Han, Y. Lu, P.H. Tan, T. Amand, B.L. Liu, B. Urbaszek, Robust optical emission polarization in MoS2 monolayers through selective valley excitation, Phys. Rev. B 86 (2014) 081301.

16. B. Radisavljevic, A. Radenovic, J. Brivio, V. Giacometti, A. Kis, Single-layer MoS_2 transistors, Nat. Nanotech. 6 (2011) 147–150.
17. B. Radisavljevic, M.B. Whitwick, A. Kis, Integrated circuits and logic operations based on single-layer MoS_2, ACS Nano 5 (2011) 9934-9938.
18. Z. Yin, H. Li, H. Li, L. Jiang, Y. Shi, Y. Sun, G. Lu, Q. Zhang, X. Chen, H. Zhang, Single-layer MoS_2 phototransistors, ACS Nano 6 (2012) 74–80.
19. H. S. Lee, S. W. Min, Y. G. Chang, M. K. Park, T. Nam, H. Kim, J. H. Kim, S. Ryu, S. Im, MoS_2 nanosheet phototransistors with thickness-modulated optical energy gap, Nano. Lett. 12 (2012) 3695–3700.
20. C. Lee, H. Yan, L. E. Brus, T.F. Heinz, J. Hone, S. Ryu, Anomalous lattice vibrations of single- and few-layer MoS_2, ACS Nano 4 (2010) 2695–2700.
21. D. Sercombe, S. Schwarz, O. Del Pozo-Zamudio, F. Liu, B.J. Robinson, E.A. Chekhovich, I.I. Tartakovskii, O. Kolosov, A.I. Tartakovskii, Optical investigation of the natural electron doping in thin MoS_2 films deposited on dielectric substrates, Sci. Rep. 3 (2013) 3489.
22. T. Kummell, W. Quitsch, S. Matthis, T. Litwin, G. Bacher, Gate control of carrier distribution in k-space in MoS_2 monolayer and bilayer crystals, Phys. Rev. B 91 (2015) 125305.
23. O. Salehzadeh, N. H. Tran, X. Liu, I. Shih, Z. Mi, Exciton Kinetics, Quantum efficiency, and efficiency drop of monolayer MoS_2 light-emitting devices, Nano Lett. 14 (2014) 4125–4130.
24. H. Nan, Z. Wang, W. Wang, Z. liang, Y. Lu, Q. Chen, D. He, P. Tan, F. Miao, X. Wang, J. Wang, Z. Ni, Strong photoluminescence enhancement of MoS_2 through defect engineering and oxygen bonding, ACS nano 8 (2014) 5738–5745.

25. G. Kresse, J. Furthmuller, Efficient iterative schemes for *ab initio* total-energy calculations using a plane-wave basis set. Phys. Rev. B 54 (1996) 11169.
26. H. J. Conley, B. Wang, J.L. Ziegler, R.F. Haglund Jr, S.T. Pantelides, K.I. Bolotin, Bandgap engineering of strained monolayer and bilayer MoS_2. Nano Lett. 13 (2013) 3626–3630.

Figure captions

Fig. 1. Optical microscopy image of the MoS_2 flake prepared by mechanical exfoliation of MoS_2. (b) Raman spectra of the 1L- and 2L-MoS_2.

Fig. 2. μ-PL spectra of 1L- and 2L-MoS2 measured at 4.2K (a) and 292 K (b). An excitation power of 1 mW/cm^2 was used. The black squares and red circles present the 1L-MoS_2 and 2L-MoS_2, respectively.

Fig. 3. PL spectra mappings of the 1L-MoS_2 at 4.2 K and 292 K (a, c) and 2L-MoS_2 at 4.2 K and 292 K (b, d) as a function of the polarizer angle. An excitation power of 3.8 kW/cm^2 was used.

Fig. 4. Polar plot of the polarized PL spectra of the 1L-MoS_2 (a) and 2L-MoS_2 (b) as a function of the polarizer angle.

Fig. 5. (a) The structure of 2L-MoS_2 including the SiO_2 substrate (2L-MoS_2 + SiO_2). The supercell is shown with a black line in the side view. Electron density distributions calculated from DFT calculations for (b) between 1L-MoS_2 and SiO_2 and (c) between 2L-MoS_2.

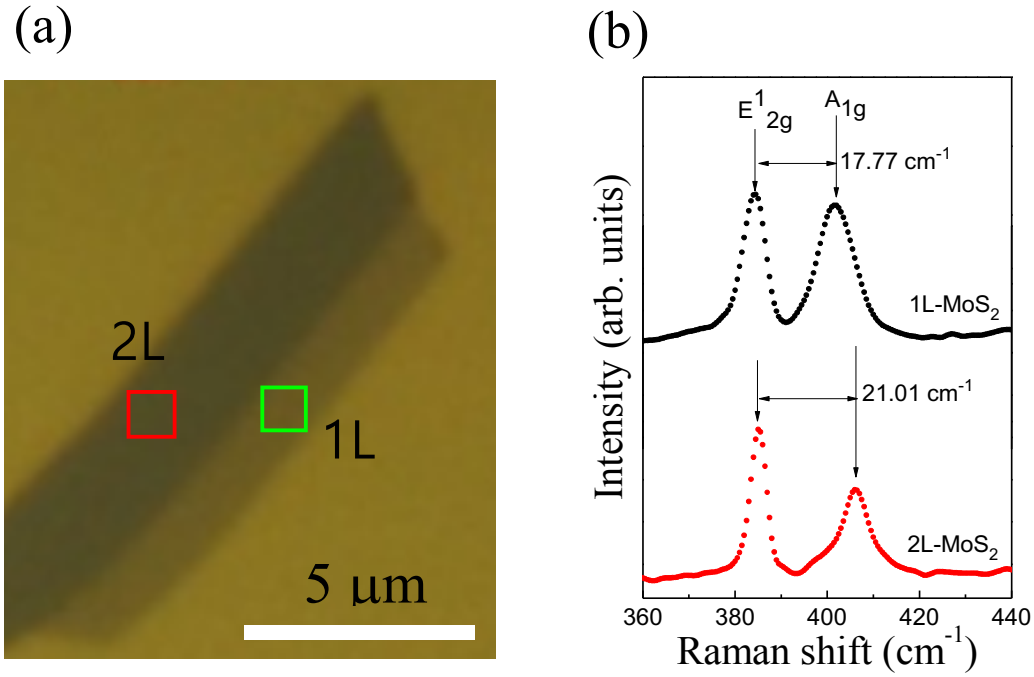
(a)
2L
1L
5 μm
(b)
E12g
A1g
17.77 cm-1
1L-MoS2
21.01 cm-1
2L-MoS2
Intensity (arb. units)
360
380
400
420
440
Raman shift (cm-1)

Fig. 1

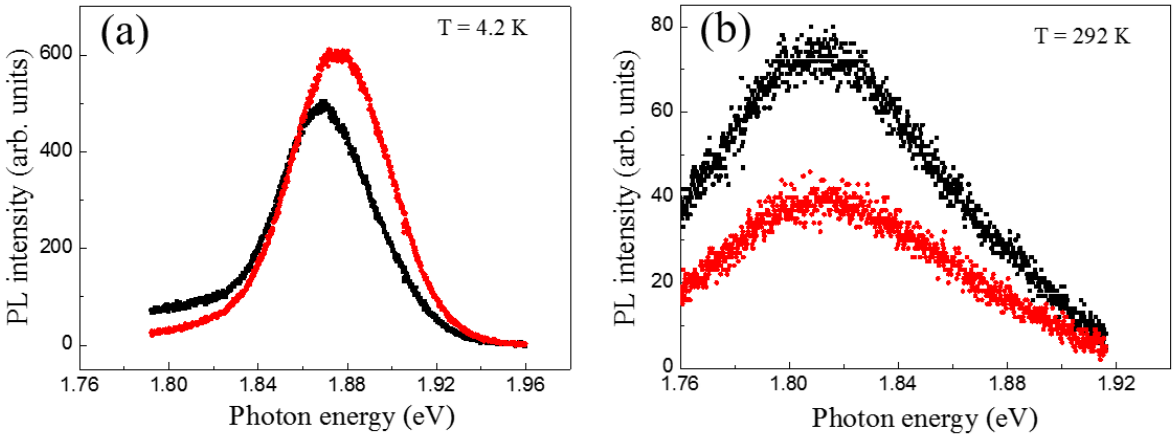
(a)
T = 4.2 K
PL intensity (arb. units)
0
200
400
600
1.76
1.80
1.84
1.88
1.92
1.96
Photon energy (eV)
(b)
T = 292 K
PL intensity (arb. units)
0
20
40
60
80
1.76
1.80
1.84
1.88
1.92
Photon energy (eV)

Fig. 2

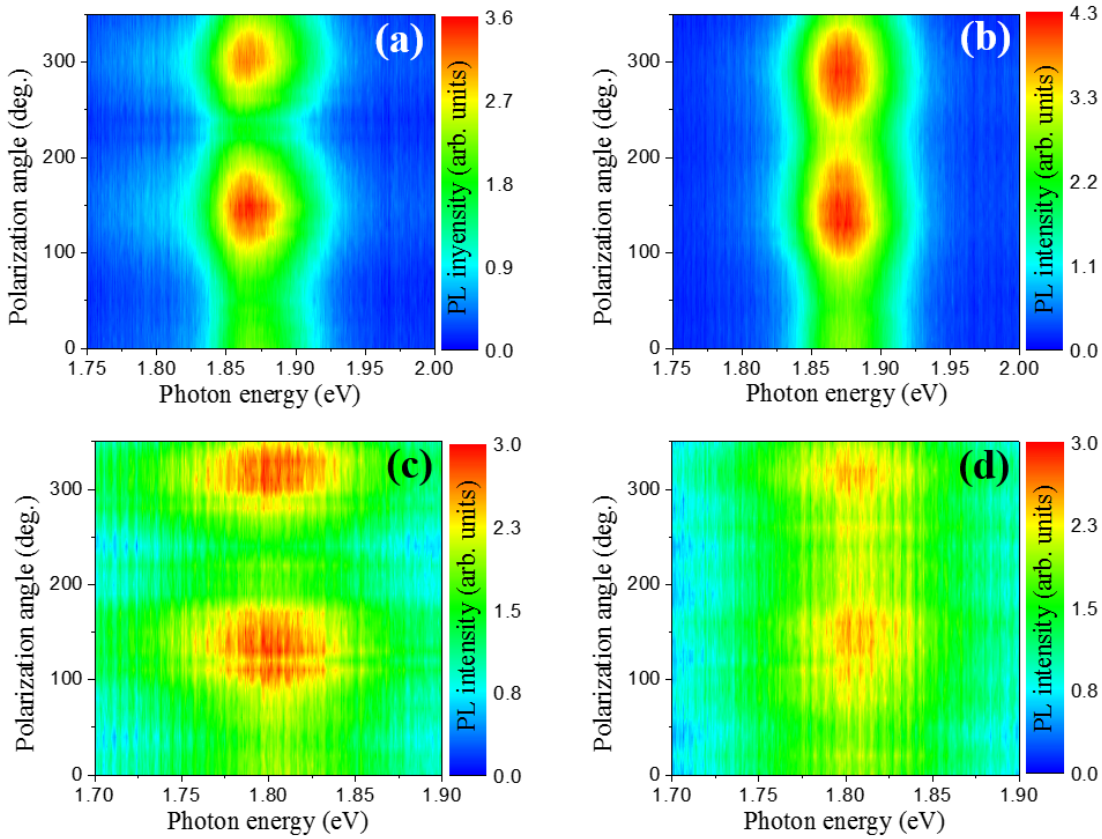
(a)
(b)
(c)
(d)
Polarization angle (deg.)
Photon energy (eV)
PL inyensity (arb. units)
PL intensity (arb. units)

Fig. 3

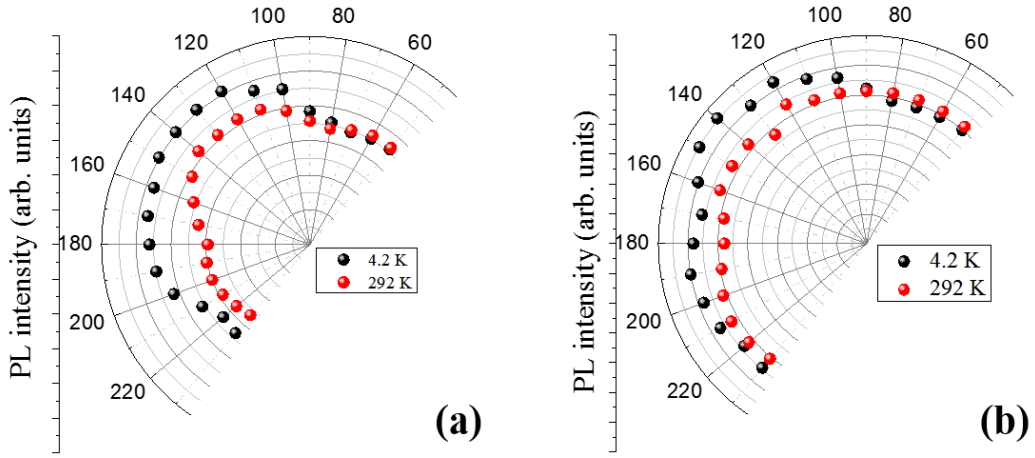
PL intensity (arb. units)
100
80
120
60
140
160
180
200
220
4.2 K
292 K
(a)
PL intensity (arb. units)
100
80
120
60
140
160
180
200
220
4.2 K
292 K
(b)

Fig. 4

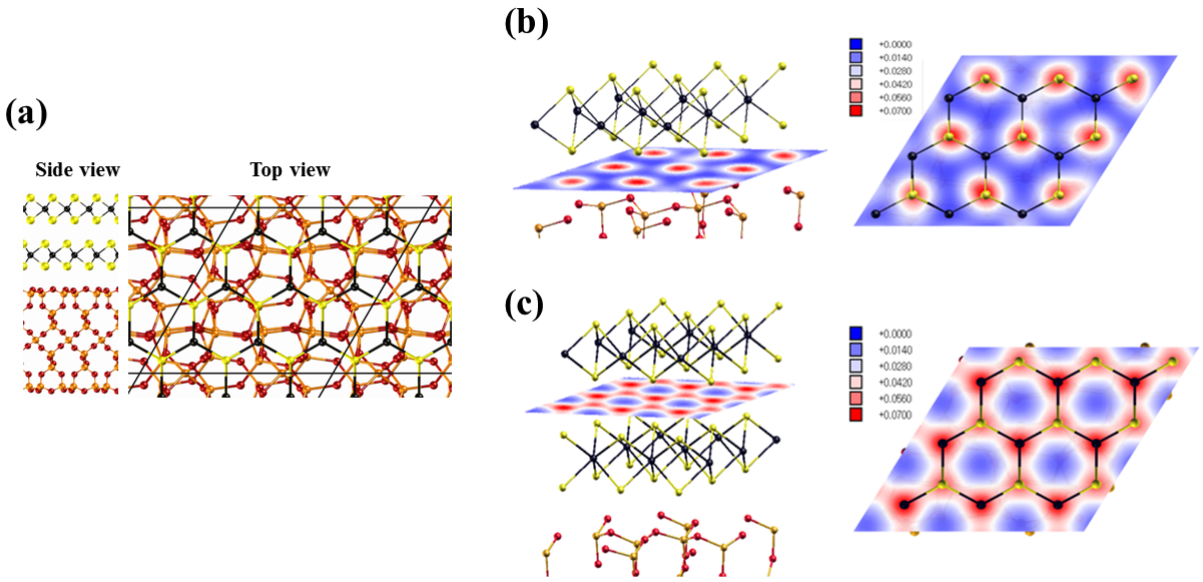
(a)
Side view
Top view
(b)
+0.0000
+0.0140
+0.0280
+0.0420
+0.0560
+0.0700
(c)
+0.0000
+0.0140
+0.0280
+0.0420
+0.0560
+0.0700

Fig. 5